A simulation study on the effect of optimized high permittivity materials on fetal imaging at 3T

van Gemert, Jeroen; Brink, Wyger M.; Remis, Rob; Webb, Andrew

DOI
10.1002/mrm.27849

Publication date
2019

Document Version
Final published version

Published in
Magnetic Resonance in Medicine

Received: 10 December 2018 | Revised: 10 May 2019 | Accepted: 19 May 2019

DOI: 10.1002/mrm.27849

FULL PAPER

Magnetic Resonance in Medicine

A simulation study on the effect of optimized high permittivity materials on fetal imaging at 3T

Jeroen van Gemert[1] | **Wyger Brink**[2] | **Rob Remis**[1] | **Andrew Webb**[2]

[1]Circuits & Systems Group, Electrical Engineering, Mathematics and Computer Science Faculty, Delft University of Technology, The Netherlands

[2]Department of Radiology, C.J. Gorter Center for High-Field MRI, Leiden University Medical Center, The Netherlands

Correspondence
Andrew Webb, Department of Radiology, C.J. Gorter Center for High-Field MRI, Leiden University Medical Center, Albinusdreef 2, 2333 ZA Leiden, The Netherlands.
Email: a.webb@lumc.nl
Twitter: @AndrewW56450446

Funding information
Dutch Technology Foundation (STW) project 13375; European Research Council Advanced Grant, Grant/Award Number: 670629 NOMA MRI.

Purpose: One of the main concerns in fetal MRI is the radiofrequency power that is absorbed both by the mother and the fetus. Passive shimming using high permittivity materials in the form of "dielectric pads" has previously been shown to increase the B_1^+ efficiency and homogeneity in different applications, while reducing the specific absorption rate (SAR). In this work, we study the effect of optimized dielectric pads for 3 pregnant models.

Methods: Pregnant models in the 3rd, 7th, and 9th months of gestation were used for simulations in a birdcage coil at 3T. Dielectric pads were optimized regions of interest (ROI) using previously developed methods for B_1^+ efficiency and homogeneity and were designed for 2 ROIs: the entire fetus and the brain of the fetus. The SAR was evaluated in terms of the whole-body SAR, average SAR in the fetus and amniotic fluid, and maximum 10 g-averaged SAR in the mother, fetus, and amniotic fluid.

Results: The optimized dielectric pads increased the transmit efficiency up to 55% and increased the B_1^+ homogeneity in almost every tested configuration. The B_1^+-normalized whole-body SAR was reduced by more than 31% for all body models. The B_1^+-normalized local SAR was reduced in most scenarios by up to 62%.

Conclusion: Simulations have shown that optimized high permittivity pads can reduce SAR in pregnant subjects at the 3rd, 7th, and 9th month of gestation, while improving the transmit field homogeneity in the fetus. However, significantly more work is required to demonstrate that fetal imaging is safe under standard operating conditions.

KEYWORDS
design tool, dielectric pad, fetal imaging, fetal MRI, high-permittivity, passive shimming

1 | INTRODUCTION

Although ultrasound remains the predominant diagnostic imaging modality for evaluating disorders related to pregnancy, fetal MRI is increasingly being used. In contrast to ultrasound, MRI visualization of the fetus is not significantly limited by maternal obesity, fetal position, or oligohydramnios; in addition, visualization of the brain is not restricted by the ossified skull. Because of its superior soft tissue contrast, MRI is able to distinguish individual fetal structures such as lung, liver, kidney, and bowel.[1] The extended FOV and ability to acquire oblique parallel slices can aid examinations of fetuses with large or complex anomalies and visualization of any lesions within the context of the entire fetal body.[2] In

particular, studies of the fetal brain and general central nervous systems (CNS) disorders are increasing in number and diagnostic quality.[3]

Fetal MRI is mainly performed at 1.5T, but there is a growing interest in 3T.[4-6] The increase in field strength results in an increase in SNR, which is beneficial because the spatial resolution can be increased and the acquisition times can be reduced. Acquiring high quality images is more challenging, however, as for higher field strength the wavelength of the RF field is reduced. Consequently, interference effects occur that may decrease the uniformity and efficiency of the RF transmit field (B_1^+), which can degrade image quality.[7-9]

Another concern in fetal MR is the amount of radiofrequency power deposited in the fetus, as well as the mother, particularly with respect to the presence of very high conductivity amniotic fluid. The allowed specific absorption rate (SAR) is defined by the International Electrotechnical Commission (IEC) standards in terms of whole-body SAR (SAR_{wb}), and head-averaged SAR. IEC 60601-2-33 suggests that pregnant women should undergo only scans that are performed in normal operating mode that limits the SAR_{wb} to 2 W/kg. Additional limits are specified for local transmit coils in terms of the local SAR (SAR_{10g}; the SAR averaged over any 10 g of tissue), limiting to 10 W/kg in the head and torso and 20 W/kg in extremities, however, these limits do not apply to body coils.

A number of previous studies have investigated via electromagnetic (EM) simulations the SAR experienced both by the mother and the fetus at 1.5T and 3T.[10-15] Hand et al.[11,12] and Pediaditis et al.[14] used a finite integration technique (FIT): the former considered a truncated model of a 28-wk pregnant woman at 1.5T and 3T, while the latter looked at a whole-body 30-wk pregnant female model at fields between 0.3T and 4T. Both studies showed that local SAR in the mother exceeded 10 W/kg before the maternal whole-body averaged SAR reached 2 W/kg. Other studies have used finite difference time domain (FDTD) methods for their simulations at 1.5T and 3T. Wu et al.[13] considered pregnant female models from 1–9 mo gestation and determined that the local SAR within the mother exceeded 10 W/kg at both field strengths in normal operating mode (i.e., 2 W/kg whole body SAR). Other studies have assessed the effects of small changes in the position of the fetus with respect to the center of the transmitting RF coil and found relatively small (<10%) differences in local SAR.[16]

Some studies have extended the SAR analysis to also estimate temperature increases within the mother and fetus[10,11] using the Pennes Bioheat equation[17] and the thermoregulation model presented by Laakso and Hirata.[18] In the most recent simulation study, Murbach et al[10] investigated the effect of using RF-shimming on a dual-transmit 3T system in terms of the SAR and temperature rise both in the mother and fetus at different gestational stages. Their general conclusions were that RF shimming can reduce the local SAR in the mother but conversely can increase the whole-body SAR and peak temperature in the fetus.

An alternative method to tailor the transmit field and SAR distribution is passive RF shimming using high permittivity materials.[19] For 3T applications, these materials typically have a relative permittivity on the order of 300–1000 and function by inducing a strong secondary magnetic field in their vicinity. Several studies performed in adults at 3T have reported a higher B_1^+ efficiency and/or homogeneity, leading to a reduced input power requirement and reduced SAR_{wb} and local SAR.[19-26] The potential benefits of using high permittivity materials in fetal MRI have been indicated previously,[27,28] but these studies did not address the full parametric design of the materials and did not take into account the different gestational stages.

In general, for passive RF shimming the dimensions, location, and constitution of the high permittivity material need to be optimized in an application-specific manner. A common approach is to perform a parametric optimization study using electromagnetic field solvers, based on a systematic trial-and-error approach. As each of these simulations involve a heterogeneous body model and a detailed model of the RF coil, such procedures typically take multiple days for a single application. In previous works, we have developed an advanced reduced order modeling technique to accelerate pad evaluations by characterizing stationary components such as the RF coil and body model in an offline-stage and compressing the resulting model. This yielded up to 4 orders of magnitude of acceleration compared to commercial software and enabled the automated design of dielectric pads in under 1 min.[29] The resulting framework is, however, body-model-specific, and optimization results obtained in a generic model are not likely to be optimal when the subject anatomy is substantially different, particularly in the case of fetal imaging.

In this paper, we use the design approach described above for a full investigation of the use of using high permittivity materials in fetal imaging at 3T. Following these modeling and optimization procedures, we design the dielectric materials to maximize B_1^+ efficiency and B_1^+ homogeneity in a specific region of interest (ROI) (i.e., the brain of the fetus and the whole fetus). In practice, the increased transmit efficiency means that less input power is needed to reach the same average B_1^+ magnitude (i.e. the same tip angle in a given imaging protocol) in the ROI than without dielectric pads. We evaluated the resulting B_1^+ fields and SAR normalized to B_1^+ in different areas of the mother and fetus for different gestational stages as well as positions within the RF coil. A sensitivity analysis was also performed to estimate the effects of realistic variations in position of the pads in a clinical setting.

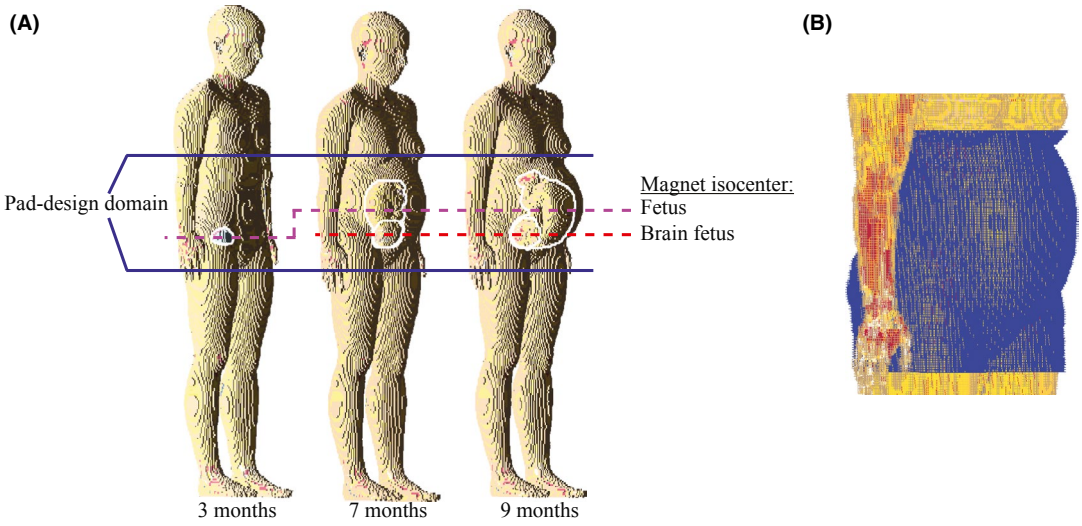

FIGURE 1 Pregnant body models in the 3rd, 7th, and 9th mo of gestation. (A) The pad design domain is the region to which every dielectric pad is confined. The imaging landmarks (the middle of the fetus and the brain of the fetus) are shown on the right side. (B) A visualization of the pad design domain (in blue) is shown for the 7th mo of gestation

2 | METHODS

2.1 | Configuration

For the EM simulations, a wide-bore high-pass birdcage body coil was used with a diameter of 750 mm, and a shield diameter of 800 mm. The shielded coil was tuned to operate in quadrature mode at a frequency of 128 MHz using 33.25 pF capacitators in the end rings. Female body models were obtained at 5 mm isotropic resolution through the Virtual Family data set[30] at the 3rd, 7th, and 9th month of gestation (with the fetus positioned head-down), and were incorporated either on a 7.5 mm or a 3.75 mm discretized uniform grid for B_1^+ field simulations and SAR evaluations, respectively. A resolution of 7.5 mm was sufficient to accurately model the B_1^+ fields, which was tested by comparing transmit efficiency and homogeneity values to those obtained using a 2.5 mm model (data not shown): the results were within 1% of each other. For the SAR simulations, a higher spatial resolution grid was used to better model the isolating material around the dielectric pad. The high permittivity materials were defined with appropriate density and electrical conductivity, to ensure proper SAR calculations and averaging. The region in which high permittivity materials can be placed, referred to as the "pad design domain," was defined as a 1.5 cm thick layer enclosing the body model from groin to breast as illustrated in Figure 1. The pregnant body models can be shifted in the body coil such that different ROIs can be positioned in the magnet isocenter. All field quantities were computed and processed using XFdtd software (v.7.4.0.3, Remcom State College, PA). The B_1^+ field quantities were normalized to 1 W input power, whereas the SAR_{10g} data were normalized to a whole-body SAR of 2 W/kg. Furthermore, normalized the B_1^+ and SAR results were normalized to the average B_1^+ magnitude achieved in the ROI when no dielectric pad is being used.

2.2 | Designing dielectric pads

An efficient forward model was used to evaluate the electromagnetic fields with a dielectric pad in place as described in Christ et al.[31] and van Gemert et al.[32] A dielectric pad design tool encompassing the methods summarized below is also freely available at https://paddesignt ool.sourceforge.io for 3T body imaging and 7T neuroimaging applications. To this end, the computational domain was divided into a domain that is stationary (i.e., containing the heterogeneous body model and RF transmit coil) and a domain that is dynamic (i.e., the pad design domain). The design domain allows defining dielectric pads with any location, geometry, and constitution, provided that the pad is confined within this domain. For every pad simulation, the stationary components remain unaffected and hence they can be characterized in advance by computing the pad-independent background fields and by constructing a so-called field response library. Subsequently, only the perturbation because of the dielectric pad on the stationary electromagnetic fields needs to be computed. As the pad design domain is small with respect to the original full computational domain, only a small problem needs to be solved and hence the computational times for dielectric pad evaluations are accelerated.

The computational times were accelerated further by applying a projection-based reduced order modeling

technique.[29] In this method, the degrees-of-freedom for the dielectric pad are restricted to reduce the solution space and the complexity of the model. For that reason, the forward model was parameterized in terms of the pad's width, height, location, and constitution by the parameter vector $\mathbf{p}$ = [ε; width; height; location]. The parameter vector also allows for the definition of 2 dielectric pads. Furthermore, the pad design domain was divided into small subdomains, on average 2.5 cm in width and 2.3 cm in height, by assigning the same material properties to grid edges that belong to a given non-overlapping subdomain. To exploit the reduced solution space because of the subdomains and the parameterization, a reduced order model was created following the procedure described in van Gemert et al.[29] In this same work, it was shown that the reduced order model produces a negligible error. This allows for field computations that are up to 4 orders of magnitude faster than conventional EM solvers such as XFdtd.

The dielectric pads were designed by optimizing the B_1^+ field in a given ROI for a certain dielectric pad parameter vector $\mathbf{p}$. The B_1^+ field was optimized as this is the primary effect of dielectric materials: the increase in transmit efficiency can then be used to reduce whole-body SAR. This was achieved by minimizing a cost function $C(\mathbf{p})$ that measures the discrepancy between the desired B_1^+ magnitude and the modeled B_1^+ magnitude within the ROI, defined as

$$C(\mathbf{p}) = \frac{1}{2}\frac{\|B_1^+(\mathbf{p}) - B_1^{+;\text{desired}}\|_{2;\text{ROI}}^2}{\|B_1^{+;\text{desired}}\|_{2;\text{ROI}}^2}, \quad (1)$$

where $B_1^{+;\text{desired}}$ is the desired B_1^+ magnitude, $B_1^+(\mathbf{p})$ is the B_1^+ magnitude because of a pad with model parameters $\mathbf{p}$, and $\|\cdot\|_{2;\text{ROI}}$ denotes the L^2 norm over the ROI. The $B_1{}^+$ efficiency is measured in units of $\mu T/\sqrt{W}$ input power, and the $B_1{}^+$ homogeneity as the coefficient of variation C_v over the ROI. The cost function was minimized using a gradient-descent method for a range of desired $|\cdot|_{2;\text{ROI}}$ magnitudes, each of which yielding a different solution in terms of transmit efficiency and C_v. With these solutions, a trade-off between homogeneity and efficiency can be made. All pad optimizations in this study were performed while fixing the pad thickness to 1.5 cm, electrical conductivity to 0.2 S/m, maximum relative permittivity to 300, and constraining the width and length of the pad to 30 cm to limit the weight of the pad.

One could consider an alternative optimization scheme in which the cost function explicitly minimizes the SAR10g in the ROI. However, this complicates the method significantly because a 10 g-averaging algorithm needs to be implemented, together with its corresponding numerical derivate, for optimization. The resulting function is not as smooth as the one used for B_1^+ efficiency, and in our experience this negatively affects the convergence and stability of the optimization.

2.3 | B_1^+ and SAR evaluation

The B_1^+ and SAR effects were evaluated for 2 ROIs: (1) the entire 3D volume of the fetus, and (2) the fetal brain only. For the 3-mo model, only the effects in the whole fetus were evaluated, as no distinction between the entire fetus and fetal brain has been made in the Virtual Family model. For each evaluation, the midpoint of the ROI was positioned at the center of the body coil. A trade-off analysis was performed by minimizing the cost function of Equation 1 for a range of desired B_1^+ magnitudes, first for a single pad and subsequently for 2 pads. The range of desired B_1^+ magnitudes considered in each of the optimizations was based on the B_1^+ magnitude without a dielectric pad, defining its lower limit, and the maximum achievable magnitude, found by running 1 optimization with a very high desired B_1^+ magnitude. A series of 8 desired B_1^+ magnitudes was then spaced linearly within this range. The pad designs that provided the optimum transmit efficiency, and the optimum field homogeneity were then analyzed in terms of SAR. The SAR distributions were evaluated in terms of SAR_{wb}, average SAR in the fetus and amniotic fluid (SAR_{avg}), and maximum 10g-averaged SAR ($SAR_{10g,max}$) within the mother, fetus, and amniotic fluid, respectively. The SAR results were normalized to the average B_1^+ magnitude in the ROI.

Finally, a sensitivity analysis was performed to determine how the transmit efficiency and homogeneity would be affected by a shift in the location of the pad from its calculated optimum, as this might occur in practice. To this end, the optimized pads were shifted by up to ~5 cm in each direction (horizontally, vertically, as well as diagonally), after which the performance metrics were compared.

3 | RESULTS

The B_1^+ field metrics resulting from the optimizations are shown in Figure 2. In all cases, a dielectric pad was obtained that improved the transmit efficiency in the ROI. Transmit efficiency gains measured ~45% in the 3-mo model, ~50% in the 7-mo model, and ~26% in the 9-mo model for both the fetal brain alone and the entire fetal volume. The C_v improved in all cases except for the 9-mo model (ROI: entire fetus). In this case, the C_v increased from 25.8% to 27.7%, while the transmit efficiency was improved by 27%. Specifications on the optimized pads can be found in Table 1, where the number of pads (1 or 2) and the pad's geometry and relative permittivity are also listed. In the majority of cases, a single dielectric pad was suggested, positioned on the anterior side of the mother. A second pad on the posterior side improved the result only in the 9-mo (ROI: brain) and 3-mo cases. The pad designs that were optimized for transmit efficiency over the entire fetus are illustrated in Figure 3.

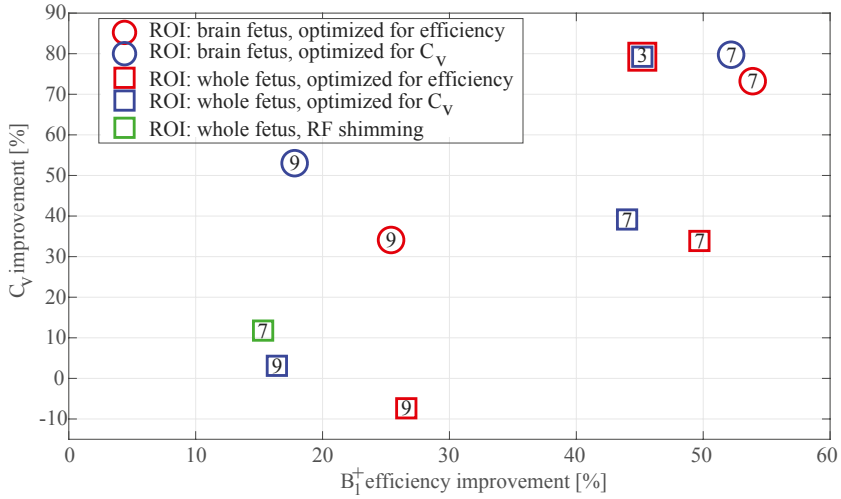

FIGURE 2 Field improvements with respect to the no dielectric pads case for the 3rd, 7th, and 9th mo of gestation. The ROI is set either to the brain of the fetus or the entire fetus. For each sweep, the optimization algorithm was run several times using different desired B_1^+ magnitudes. The symbols indicate the cases that gave the maximum C_v improvement and the maximum transmit efficiency improvement, respectively. The green square shows the result obtained from the work from Murbach et al.,[10] where RF shimming is being used

TABLE 1 Summary of the B_1^+ transmit efficiency gains and the C_v realized by the optimized dielectric pads

Configuration	Transmit efficiency (μT/√W)	C_v (%)	Anterior pad	Posterior pad
9 mo				
ROI: fetal brain				
No dielectric pads	0.143	13.9		
Pad best B_1^+ efficiency	0.179 (+25.4%)	9.16	$\varepsilon_r = 300$, $18.2 \times 27.9 \times 1.5$ cm^3	$\varepsilon_r = 281$, $29.4 \times 26.6 \times 1.5$ cm^3
Pad best C_v	0.168 (+17.8%)	6.53	$\varepsilon_r = 300$, $18.1 \times 25.6 \times 1.5$ cm^3	$\varepsilon_r = 300$, $18.0 \times 27.9 \times 1.5$ cm^3
ROI: entire fetus				
No dielectric pads	0.109	25.8		
Pad best B_1^+ efficiency	0.138 (+26.6%)	27.7	$\varepsilon_r = 300$, $29.2 \times 29.2 \times 1.5$ cm^3	
Pad best C_v	0.127 (+16.4%)	25.0	$\varepsilon_r = 248$, $24.7 \times 29.2 \times 1.5$ cm^3	
7 mo				
ROI: fetal brain				
No dielectric pads	0.161	15.8		
Pad best B_1^+ efficiency	0.248 (+53.9%)	4.23	$\varepsilon_r = 300$, $29.3 \times 28.3 \times 1.5$ cm^3	
Pad best C_v	0.245 (+52.2%)	3.20	$\varepsilon_r = 300$, $29.3 \times 28.3 \times 1.5$ cm^3	
ROI: entire fetus				
No dielectric pads	0.131	18.9		
Pad best B_1^+ efficiency	0.196 (+49.7%)	12.5	$\varepsilon_r = 300$, $29.2 \times 29.9 \times 1.5$ cm^3	
Pad best C_v	0.189 (+44.0%)	11.5	$\varepsilon_r = 270$, $29.2 \times 29.9 \times 1.5$ cm^3	
3 mo				
ROI: entire fetus				
No dielectric pads	0.209	8.05		
Pad best B_1^+ efficiency and C_v	0.303 (+45.2%)	1.67	$\varepsilon_r = 257$, $24.9 \times 15.6 \times 1.5$ cm^3	$\varepsilon_r = 300$, $29.4 \times 29.3 \times 1.5$ cm^3

The ROI is set to either the fetal brain or the entire fetus and the midpoint of the ROI is positioned in the isocenter of the body coil. Results are compared for the dielectric pad that optimized either the B_1^+ efficiency or homogeneity, except for the 3 mo case where both designs coincided. All quantities were normalized to 1 W input power.

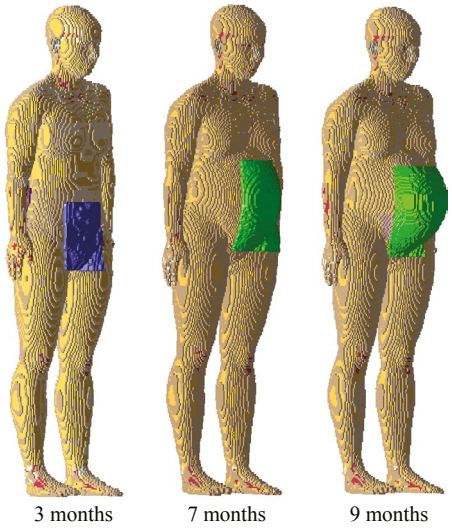

FIGURE 3 Design of the dielectric pads. The design is shown for the optimum dielectric pads that provided the best transmit efficiency for the ROI set to the entire fetus

The B_1^+ fields and the SAR_{10g} distributions for the optimized pads are illustrated in Figures 4 and 5, and Figures 6 and 7, respectively, for the 7th and 9th months of gestation. The results for the 3rd month of gestation can be found Supporting Information Figure S1. The Maximum SAR_{10g} values are summarized in Table 2 (including the results for the pads that provided the minimum C_v). For the SAR_{wb} normalized case, the spatial pattern of the SAR_{10g} was quite similar to that without dielectric pads, which is consistent with previous studies.[20,23,25] In the 3rd and 6th column of Figures 6 and 7, the B_1^+ normalized SAR_{10g} data is shown for the case with dielectric pads, indicating a substantial reduction in peak local SAR throughout the configuration.

For all SAR evaluations, a decrease in SAR_{wb} was observed when optimized pads are in place. Specifically, the SAR_{wb} was reduced by more than 53%, 55%, and 31% for the 3rd, 7th, and 9th months of gestation, respectively. For the pads that minimized C_v, the reductions in SAR_{wb} were slightly lower (i.e., 53%, 51% and 23%). The SAR_{avg} and

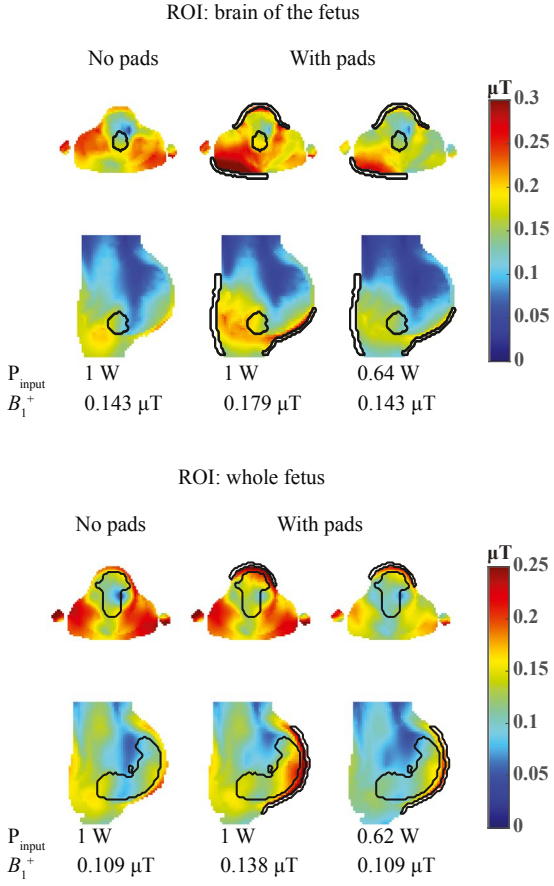

FIGURE 4 B_1^+ fields for the 9th mo of gestation. The cross-sections shown are obtained through the midpoint of the ROI. The 1st and 2nd column are normalized to 1 W input power. The 3rd column is normalized for B_1^+ (i.e., the same B_1^+ magnitude is achieved within the ROI as in the case without dielectric pads). For an equal B_1^+ magnitude within the ROI, the input power is reduced in all configurations

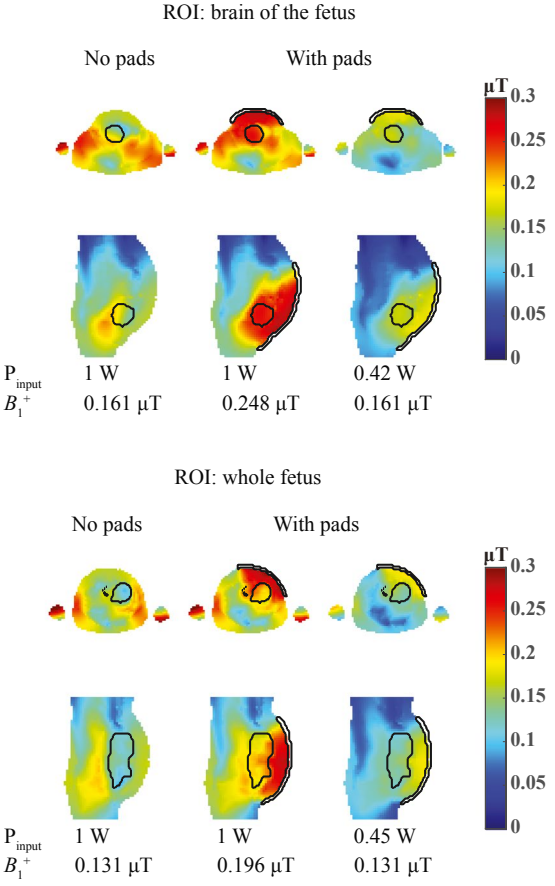

FIGURE 5 B_1^+ fields for the 7th mo of gestation. The cross-sections shown are obtained through the midpoint of the ROI. The 1st and 2nd column are normalized to 1 W input power. The 3rd column is normalized for B_1^+ (i.e., the same B_1^+ magnitude is achieved within the ROI as in the case without dielectric pads). For an equal B_1^+ magnitude within the ROI, the input power is reduced in all configurations

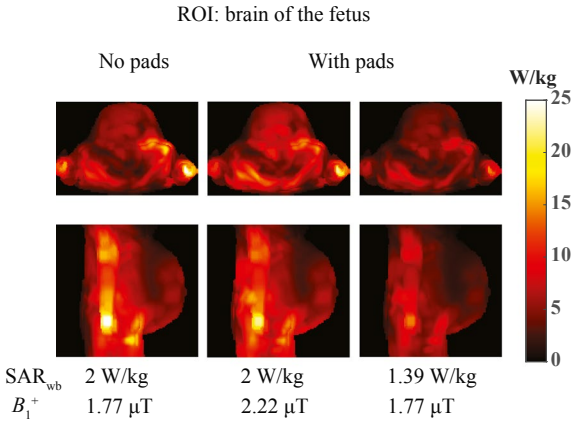

FIGURE 6 Maximum intensity projections of the SAR_{10g} evaluated for the 9th mo of gestation. The 1st and 2nd column are normalized to $SAR_{wb} = 2$ W/kg. The 3rd column is normalized for B_1^+ (i.e., the same B_1^+ magnitude is achieved within the ROI as in the case without dielectric pads). For an equal B_1^+ magnitude within the ROI, SAR_{10g} is reduced in all configurations

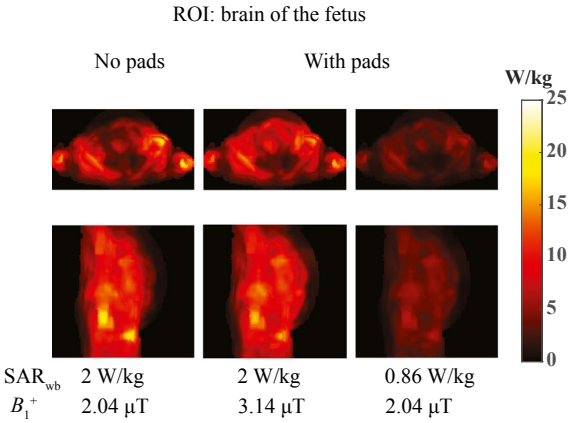

FIGURE 7 Maximum intensity projections of the SAR_{10g} evaluated for the 7th mo of gestation. The 1st and 2nd column are normalized to $SAR_{wb} = 2$ W/kg. The 3rd column is normalized for B_1^+ (i.e., the same B_1^+ magnitude is achieved within the ROI as in the case without dielectric pads). For an equal B_1^+ magnitude within the ROI, SAR_{10g} is reduced in all configurations

$SAR_{10g,max}$ were reduced in almost all cases, except for the 9-mo case where the pad was optimized to achieve a minimum C_v. Here, an increased $SAR_{10g,max}$ in the fetus of 6–14% was seen. The largest reductions in SAR are generally observed in the mother. For the 9-mo model, the amniotic fluid showed intermediate reductions in SAR_{avg}, and only small variations were observed in the fetus. In the other 2 models, similar gains were observed in the fetus and the amniotic fluid.

The results from the sensitivity analysis are shown in Table 3. The performance metrics of the optimized dielectric pads are quite robust to small changes in the optimum location of the pad (up to 5 cm in each direction), which is consistent with previous findings. Except for the 9 mo gestational age (ROI set to the entire fetus), the dielectric pads still improve the efficiency and field homogeneity with respect to the no dielectric pads case.

4 | DISCUSSION AND CONCLUSIONS

In this study, the effects of optimized dielectric pads on the B_1^+ field and associated SAR in fetal imaging at 3T have been simulated. The SAR evaluation in this work is based on the practical situation in which the same imaging protocol is run for the cases with and without the dielectric pad (i.e., the same average B_1^+ value is realized in both scans). This means that the SAR values reported should be normalized to the average B_1^+ value within the particular ROI. The results show that, in general, considerable increases in both simulated transmit efficiency and homogeneity as well as reductions in whole-body and local B_1^+ -normalized SAR can be obtained using optimized dielectric pads, suggesting an improved safety of fetal imaging at 3T.

In the current design study, for practical reasons, both the dimensions as well as the relative permittivity of the

TABLE 2 Summary of the SAR evaluations

Configuration	SAR_{wb} (W/kg)	SAR_{avg} (W/kg)		$SAR_{10g,max}$ (W/kg)		
	Mother	Fetus	Amniotic	Mother	Fetus	Amniotic
9 mo						
ROI: fetal brain						
No dielectric pads	2.00	1.04	2.65	25.4	7.11	15.3
Pad best B_1^+ efficiency	1.39 (−31%)	0.88 (−15%)	1.90 (−28%)	15.6 (−38%)	6.49 (−9%)	10.1 (−34%)
Pad best C_v	1.55 (−23%)	1.03 (−1%)	2.22 (−16%)	18.4 (−27%)	8.13(+14%)	10.8 (−30%)
ROI: entire fetus						
No dielectric pads	2.00	1.01	2.80	29.3	7.48	15.1
Pad best B_1^+ efficiency	1.15 (−42%)	0.92 (−9%)	2.08 (−26%)	15.6 (−47%)	6.75 (−10%)	8.08 (−47%)
Pad best C_v	1.47 (−27%)	1.04 (+3%)	2.52 (−10%)	19.4 (−34%)	7.91 (+6%)	12.0 (−20%)
7 mo						
ROI: fetal brain						
No dielectric pads	2.00	2.00	4.35	19.8	12.8	13.7
Pad best B_1^+ efficiency	0.86 (−57%)	1.18 (−41%)	2.66 (−39%)	7.47 (−62%)	5.54 (−57%)	6.01 (−56%)
Pad best C_v	0.88 (−56%)	1.24 (−38%)	2.80 (−36%)	7.73 (−61%)	5.93 (−54%)	6.41 (−53%)
ROI: entire fetus						
No dielectric pads	2.00	2.32	5.02	24.4	14.9	16.1
Pad best B_1^+ efficiency	0.91 (−55%)	1.48 (−36%)	3.50 (−30%)	8.88 (−64%)	7.79 (−48%)	8.52 (−47%)
Pad best C_v	0.98 (−51%)	1.57 (−32%)	3.64 (−28%)	9.73 (−60%)	8.30 (−44%)	9.09 (−44%)
3 mo						
ROI: entire fetus						
No dielectric pads	2.00	1.6	1.32	22.1	2.68	2.91
Pad best B_1^+ efficiency and C_v	0.94 (−53%)	1.33 (−17%)	1.13 (−14%)	9.66 (−56%)	2.03 (−24%)	2.04 (−30%)

The ROI is set to the fetal brain or the entire fetus and the midpoint of the ROI is positioned in the magnet isocenter. SAR values for the no dielectric pads case are normalized to a SAR_{wb} of 2 W/kg. The dielectric pad cases are normalized to the average B_1^+ magnitude in the ROI obtained when no dielectric pads are used (i.e., the same B_1^+ magnitude is reached in the ROI). All percentages in the SAR_{wb}, SAR_{avg}, and $SAR_{10g,max}$ columns are with respect to the original configuration (i.e., where no dielectric pads are being used).

TABLE 3 Sensitivity analysis of the dielectric pad with respect to the B_1^+ transmit efficiency gains and the C_v realized by the optimized dielectric pads

Configuration	Shift of ~2.5 cm		Shift of ~5 cm	
	Worst case transmit efficiency degradation (%)	Worst case C_v (%)	Worst case transmit efficiency degradation (%)	Worst case C_v (%)
9 mo				
ROI: fetal brain	5.6	10.7	8.1	13.5
ROI: entire fetus	7.4	28.4	12.9	28.4
7 mo				
ROI: fetal brain	5.0	6.9	13.7	10.4
ROI: entire fetus	6.0	15.7	9.6	18.6
3 mo				
ROI: entire fetus	6.7	3.4	11.4	5.6

The ROI is set to either the fetal brain or the entire fetus and the midpoint of the ROI is positioned in the isocenter of the body coil. A spatial shift is applied in all directions of ~2.5 cm and 5 cm. The worst case transmit efficiency degradation is depicted and the maximum obtained C_v.

pad were restricted. Higher transmit efficiency gains are attainable when we relax these constraints. For example, the transmit efficiency can be increased by up to 36% for the 9-mo (ROI: fetus) model instead of the 27% reported here, however, this would require a dielectric pad exceeding 15 kg in weight. Our constraints ensure that the weight of the dielectric pad stays below 4 kg, which is considered a suitable limit to preserve subject comfort based on previous experience at our institute.

The possibility of using a universal pad for imaging the whole fetus for all 3 studied gestational ages was also investigated. Therefore, the optimal pad that was found in the 7- and 9-mo models (that were identical except for their location) was also used for the 3-mo model. This resulted in a small compromise compared to the optimum design (i.e., the B_1^+ efficiency gain decreased from 45.2% to 42.7%, and the C_v increases from 1.7% to 6.9%).

It should be noted that, compared to the study of Murbach et al.,[10] different SAR results were found for the 7-mo configuration where no shimming is applied and where no dielectric pads are used. Specifically, the SAR_{10g} in the fetus and amniotic fluid reached values that were twice as low as compared to our study. These differences may be caused by differences in either the coil model or the subject meshing; our pregnant models were limited to a uniform and isotropic spatial resolution of 5 mm, whereas the model from Murbach et al.[10] supported a higher spatial resolution. These differences should, however, not change the conclusions with respect to the relative effects of the dielectric materials, which are independent from the reference model.

IEC 60601-2-33 suggests that pregnant women should only undergo scans that are performed in normal operating mode that limits the SAR_{wb} to 2 W/kg. However, whether this normal operational mode is in fact safe in terms of the local tissue temperature is a concern also raised in the context of RF shimming by Murbach et al.[10] and certainly needs much further investigation in the context of dielectric shimming as well. In addition, the fact that the body models used on the MR scanners themselves to calculate SAR do not accurately reflect the anatomy of pregnancy at different stages is another concern that needs to be investigated more thoroughly. Therefore, although the current work shows that dielectric pads reduce the B_1^+-normalized SAR10 g for a given model, and provided that identical imaging parameters are used in a fixed imaging protocol the safety is improved, this should in no way be construed as a general statement that fetal imaging is "safe" at 3 T.

With respect to future work on dielectric pads, the anatomic body model used in this study is currently limited to a 5-mm isotropic resolution: this is currently restricted by the availability of higher resolution anatomic models only for specific electromagnetic modeling platforms. Although this resolution is sufficient for local SAR assessment at 3T (see e.g., Homann et al.),[33] it would be an improvement to this pad design study to also incorporate finer anatomic details. Furthermore, the number of pregnant body models was limited to 3, because others are currently not available. This would help to answer more definitively the question of how effective a single or perhaps 2 or 3 "universal" pads would be for different gestational stages, rather than considering patient-specific designs. The incorporation of different thermal models to estimate temperature increases during scanning is also an important aspect of future work, although again, this is currently somewhat limited by the small number of human body models available.

In conclusion, we have shown in simulations that optimized high permittivity pads can improve the transmit field homogeneity and efficiency in the fetus and also reduce the B_1^+-normalized SAR in the 3rd, 7th, and 9th mo of gestation.

ACKNOWLEDGMENTS

This project was funded by the Dutch Technology Foundation (STW) project 13375 and the European Research Council Advanced grant 670629 NOMA MRI.

REFERENCES

1. Frates MC, Kumar AJ, Benson CB, Ward VL, Tempany CM. Fetal anomalies: comparison of MR imaging and US for diagnosis. *Radiology*. 2004;232:398–404.
2. Saleem SN. Fetal MRI: an approach to practice: a review. *J Adv Res*. 2014;5:507–523.
3. Manganaro L, Bernardo S, Antonelli A, Vinci V, Saldari M, Catalano C. Fetal MRI of the central nervous system: state-of-the-art. *Eur J Radiol*. 2017;93:273–283.
4. Krishnamurthy U, Neelavalli J, Mody S, et al. MR imaging of the fetal brain at 1.5T and 3.0T field strengths: comparing specific absorption rate (SAR) and image quality. *J Perinat Med*. 2015;43:209–220.
5. Weisstanner C, Gruber GM, Brugger PC, et al. Fetal MRI at 3T—ready for routine use? *Br J Radiol*. 2017;90:20160362.
6. Victoria T, Johnson AM, Edgar JC, Zarnow DM, Vossough A, Jaramillo D. Comparison between 1.5-T and 3-T MRI for fetal imaging: is there an advantage to imaging with a higher field strength? *AJR Am J Roentgenol*. 2016;206:195–201.
7. Bernstein MA, Huston J, Ward HA. Imaging artifacts at 3.0 T. *J Magn Reson Imaging*. 2006;24:735–746.
8. Chang KJ, Kamel IR. Abdominal imaging at 3T: challenges and solutions. *Appl Radiol*. 2010;39:22.
9. Dietrich O, Reiser MF, Schoenberg SO. Artifacts in 3-T MRI: physical background and reduction strategies. *Eur J Radiol*. 2008;65:29–35.
10. Murbach M, Neufeld E, Samaras T, et al. Pregnant women models analyzed for RF exposure and temperature increase in 3T RF shimmed birdcages. *Magn Reson Med*. 2017;77:2048–2056.
11. Hand JW, Li Y, Hajnal JV. Numerical study of RF exposure and the resulting temperature rise in the foetus during a magnetic resonance procedure. *Phys Med Biol*. 2010;55:913–930.

12. Hand JW, Li Y, Thomas EL, Rutherford MA, Hajnal JV. Prediction of specific absorption rate in mother and fetus associated with MRI examinations during pregnancy. *Magn Reson Med*. 2006;55:883–893.
13. Wu D, Shamsi S, Chen J, Kainz W. Evaluations of specific absorption rate and temperature increase within pregnant female models in magnetic resonance imaging birdcage coils. *IEEE Trans Microw Theory Tech*. 2006;54:4472–4478.
14. Pediaditis M, Leitgeb N, Cech R. RF-EMF exposure of fetus and mother during magnetic resonance imaging. *Phys Med Biol*. 2008;53:7187–7195.
15. Murbach M, Cabot E, Neufeld E, et al. Local SAR enhancements in anatomically correct children and adult models as a function of position within 1.5 T MR body coil. *Prog Biophys Mol Biol*. 2011;107:428–433.
16. Saito K, Kikuchi S, Takahashi M, Ito K, Ikehira H. SAR estimations of pregnant woman during MR imaging for abdomen by numerical calculations. In Proceedings of the 18th International Zurich Symposium on Electromagnetic Compatibility, Munich, Germany, 2007. p. 45–48.
17. Pennes HH. Analysis of tissue and arterial blood temperatures in the resting human forearm. *J Appl Physiol*. 1948;1:93–122.
18. Laakso I, Hirata A. Dominant factors affecting temperature rise in simulations of human thermoregulation during RF exposure. *Phys Med Biol*. 2011;56:7449–7471.
19. Yang QX, Wang J, Wang J, Collins CM, Wang C, Smith MB. Reducing SAR and enhancing cerebral signal-to-noise ratio with high permittivity padding at 3 T. *Magn Reson Med*. 2011;65:358–362.
20. de Heer P, Brink WM, Kooij BJ, Webb AG. Increasing signal homogeneity and image quality in abdominal imaging at 3 T with very high permittivity materials. *Magn Reson Med*. 2012;68:1317–1324.
21. Luo W, Lanagan MT, Sica CT, et al. Permittivity and performance of dielectric pads with sintered ceramic beads in MRI: early experiments and simulations at 3 T. *Magn Reson Med*. 2013;70:269–275.
22. Yang QX, Rupprecht S, Luo W, et al. Radiofrequency field enhancement with high dielectric constant (HDC) pads in a receive array coil at 3.0T. *J Magn Reson Imaging*. 2013;38:435–440.
23. Brink WM, Webb AG. High permittivity pads reduce specific absorption rate, improve B 1 homogeneity, and increase contrast-to-noise ratio for functional cardiac MRI at 3 T. *Magn Reson Med*. 2014;71:1632–1640.
24. Brink WM, van den Brink JS, Webb AG. The effect of high-permittivity pads on specific absorption rate in radiofrequency-shimmed dual-transmit cardiovascular magnetic resonance at 3T. *J Cardiovasc Magn Reson*. 2015;17:82.
25. Winkler SA, Rutt BK. Practical methods for improving B1+ homogeneity in 3 Tesla breast imaging. *J Magn Reson Imaging*. 2015;41:992–999.
26. Brink WM, Versluis MJ, Peeters JM, Börnert P, Webb AG. Passive radiofrequency shimming in the thighs at 3 Tesla using high permittivity materials and body coil receive uniformity correction. *Magn Reson Med*. 2016;76:1951–1956.
27. Luo M, Hu C, Zhuang Y, Chen W, Liu F, Xin SX. Numerical assessment of the reduction of specific absorption rate by adding high dielectric materials for fetus MRI at 3 T. *Biomed Tech (Berl)*. 2016;61:455–461.
28. Luo C, Li N, Xie G, Zhang X, Liu X, Li Y. Assessment of high dielectric material in different sizes for fetal MRI at 3T. In Proceedings of the 26th Annual Scientific Meeting of the ISMRM, Paris, France, 2018. p. 4188.
29. van Gemert J, Brink WM, Webb AG, Remis RF. High-permittivity pad design for dielectric shimming in magnetic resonance imaging using projection-based model reduction and a nonlinear optimization scheme. *IEEE Trans Med Imaging*. 2018;37:1035–1044.
30. Christ A, Kainz W, Hahn EG, et al. The virtual family—development of surface-based anatomical models of two adults and two children for dosimetric simulations. *Phys Med Biol*. 2010;55:N23–N38.
31. van Gemert J, Brink W, Webb A, Remis R. An efficient methodology for the analysis of dielectric shimming materials in magnetic resonance imaging. *IEEE Trans Med Imaging*. 2017;36:666–673.
32. Brink WM, Remis RF, Webb AG. A theoretical approach based on electromagnetic scattering for analysing dielectric shimming in high-field MRI. *Magn Reson Med*. 2016;75:2185–2194.
33. Homann H, Börnert P, Eggers H, Nehrke K, Dössel O, Graesslin I. Toward individualized SAR models and in vivo validation. *Magn Reson Med*. 2011;66:1767–1776.

SUPPORTING INFORMATION

Additional supporting information may be found online in the Supporting Information section at the end of the article.

FIGURE S1 B_1^+ fields and maximum intensity projections of the SAR_{10g} for the 7th mo of gestation. The cross-sections shown are obtained through the midpoint of the ROI. In (A), the 1st and 2nd column are normalized to 1 W input power, whereas in (B), it is normalized to $SAR_{wb} = 2$ W/kg. The 3rd column is normalized for B_1^+ (i.e., the same B_1^+ magnitude is achieved within the ROI as in the case without dielectric pads). For an equal B_1^+ magnitude within the ROI the input power and SAR_{10g} is reduced in all configurations

How to cite this article: van Gemert J, Brink W, Remis R, Webb A. A simulation study on the effect of optimized high permittivity materials on fetal imaging at 3T. *Magn Reson Med*. 2019;82:1822–1831.
https://doi.org/10.1002/mrm.27849